# Impact Modification of Poly(trimethylene terephthalate)/ Polypropylene Blend Nanocomposites: Fabrication and Characterization

**Dinesh Upadhyay, Smita Mohanty, Sanjay K. Nayak, M. Rahail Parvaiz, Bishnu P. Panda**

*Laboratory for Advanced Research in Polymeric Materials, Central Institute of Plastic Engineering and Technology, Bhubaneswar 751024, India*

Received 10 August 2009; accepted 25 July 2010
DOI 10.1002/app.33106
Published online 8 November 2010 in Wiley Online Library (wileyonlinelibrary.com).

**ABSTRACT:** A poly(trimethylene terephthalate) (PTT)/ polypropylene (PP) blend and the nanocomposites were prepared with and without the addition of a compatibilizer precursor [maleic anhydride grafted polypropylene (MAPP)]. A reactive route was used for the compatibilization with the addition of MAPP during melt blending in a batch mixer. Organically modified nanoclays were used as nanoscale reinforcements to prepare the blend nanocomposites. Mechanical tests revealed optimum performance characteristics at a PTT/PP blend ratio of 80 : 20. Furthermore, incorporation of nanoclays up to 3 wt % showed a higher impact strength and higher tensile strength and modulus in the blend nanocomposites compared to the optimized blend. The nanocomposite formation was established through X-ray diffraction and transmission electron microscopy (TEM). Thermal measurements were carried out with differential scanning calorimetry (DSC) and thermogravimetric analysis (TGA). DSC thermograms revealed an increase in the crystallization temperature in the presence of the nanoclays in the blend system containing Cloisite 30B. TGA thermograms also indicated that the thermal stability of blend increased with the incorporation of Cloisite 30B. Furthermore, dynamic mechanical analysis measurements showed that the Cloisite 30B nanocomposite had the maximum modulus compared to other nanocomposites. TEM micrographs confirmed an intercalated morphology in the blend nanocomposites. © 2010 Wiley Periodicals, Inc. J Appl Polym Sci 120: 932–943, 2011

**Key words:** blending; compatibilization; differential scanning calorimetry (DSC); mechanical properties; nanocomposites

## INTRODUCTION

The blending of two or more polymers has emerged as an established route for the design of tailor-made polymeric materials with desired attributes for various high-performance applications.[1–4] However, most polymer pairs are inherently immiscible; this results in incompatibility with subsequent phase separation in the blend matrix. The microstructure and morphology in the blends also play a vital role in controlling the final properties, thereby widening the technological applications of the blends.[5]

The mechanical properties of a blend or an alloy are determined not only by the properties of its individual components but also by its phase morphology and interphase adhesion.[6] The applications of immiscible blends are often limited because the adhesion strength at the interface is not strong enough to attain a stable morphology. The use of a suitable compatibilizer, copolymers, or grafting agents has been reported to improve the interaction between the two blend components at the interface. Reactive compatibilization leads to the modification of the interfaces between two-phase blends; this results in a phase structure with synergism in the properties[7] suitable for particular end-use applications. One of the important effects of compatibilizers is the reduction of the interfacial tension in the melt; this causes an emulsifying effect and leads to a good dispersion of one phase in the other. The second major effect is an increase in the adhesion at the phase boundaries; this gives improved stress transfer. More recently, the addition of layered silicates into the blend matrix has been reported, wherein the organoclays themselves act as a compatibilizing agent to reduce the particle size of the matrix polymer dispersed in the base matrix of the blend.[8,9] Layered silicates, with their inherently high aspect ratio, which ranges from 1000 to 2000, offer more surface contact per unit filler within the polymer matrix; this results in enhanced performance characteristics.[10] With a minimum organoclay loading of 1%, a nearly 10% increase in the mechanical properties has been reported. Blend nanocomposites of a variety of polymers, such as polypropylene (PP)/ethylene octene comonomer, PP/ polyamide, polystyrene/poly(methyl methacrylate), and poly(propylene oxide)/polyamide 6, synthesized by different techniques, such as *in situ* intercalation,

*Correspondence to:* S. K. Nayak (drsknayak@gmail.com).

melt intercalation, and solution intercalation, have already been reported by several researchers.[11–15]

The primary objective of this study was to fabricate compatibilized blends and blend nanocomposites of poly(trimethylene terephthalate) (PTT) and PP with the melt-blending technique. Also, the details of the effects of the addition of compatibilizer and nanoclay on the morphology and mechanical and thermal behaviors of the blends and nanocomposites were investigated.

## EXPERIMENTAL

### Materials

PTT (Futura CPTT) was purchased from Futura Polymers, Ltd. (Chennai, India); it had a density of 1.3 g/cm$^3$ and intrinsic viscosity of 0.915 dL/g (phenol/carbon tetrachloride = 60 : 40). PP (Halene-P, M110) was obtained from Haldia Petrochemicals, Ltd. (Haldia, India); it had a melt flow index of 11 g/10 min. The clay minerals were commercially available: Cloisite 20A (C20A; cation-exchange capacity = 95 mequiv/100 g), which was a clay treated with the organic modifier dimethyl dihydrogenated tallow ammonium, and Cloisite 30B (C30B; cation-exchange capacity = 90 mequiv/100 g of clay), which was a clay organically treated with methyl tallow bis-2-hydroxylethyl ammonium (Southern Clay Products, Inc., USA). Maleic anhydride grafted polypropylene (MAPP; Epolene G-3003), with a density of 0.9 g/cc and an acid number of 47, was purchased from Eastman Chemicals., Mumbai, India.

### Preparation of the PTT/PP blends and nanocomposites

Blends of PTT and PP at various compositions (90 : 10, 80 : 20, 70 : 30, 50 : 50, and 30 : 70 w/w) were prepared with a batch mixer (Torque Rheocord-9000 Haake, Karlsruhe, Germany) at a screw speed of 60 rpm and temperature of 230°C for a duration of 5 min. Before blending, PTT was predried at 120°C for 24 h. PTT, PP, and MAPP were mixed simultaneously during blending. Specimens were prepared with a compression press at 240°C with a pressure of 48 kg/cm$^3$, a heating time of 7 min, breathing times of 0.5 min (three times), and a cooling time of 12 min.

The blend composition was optimized at an 80 : 20 ratio of PTT to PP and was maintained for the preparation of the polymer blend nanocomposites at 3 wt % nanoclay with a similar fabrication technique to that reported previously.

### Morphological characterization

Transmission electron microscopy (TEM) was performed on a TEM analyzer (JEOL, JEM 1400, Tokyo, Japan) operated at an accelerating voltage of 200 kV. Before TEM imaging, thin cross sections of the nanocomposite were prepared, cryotomed, and stained for at least 24 h. The chamber was kept at −170°C with a Dewar filled with liquid $N_2$ during sectioning. We used a Leica Ultracut UCT-GA-D/E-100 ultramicrotome (Wetzlar, Germany) as a glass knife. The sections were then stained with a saturated solution of uranyl acetate and counterstained with 4% lead citrate. The samples were then ready for examination by TEM. After image exposure, the film was developed in the dark room with the specified procedure. The dry negatives were scanned onto a computer and saved at their original size at the highest resolution possible and then analyzed. Scanning electron microscopy (SEM) observations of the impact-fractured specimens were carried out with a Hitachi S-3400 N (Tokyo, Japan) at an accelerated voltage of 15 kV. The samples were fractured under cryogenic conditions and gold sputtered before analysis. The wide-angle X-ray diffraction (WAXD) patterns were obtained with a Phillips X'Pert X-ray diffractometer (40 kV, 30 mA equipped with a Cu K$\alpha$ radiation source, wavelength = 1.54 Å). The diffraction pattern of nanoclays and the blend nanocomposites were examined. Fourier transform infrared (FTIR) spectra of the PTT/PP blend and the nanocomposites were recorded with a Nicolet 6700 spectroscope (Thermo Electron Corp., USA). Each spectrum was obtained by the coaddition of 64 consecutive scans with a resolution of 4 cm$^{-1}$ within the range 500–4000 cm$^{-1}$.

### Mechanical properties

The tensile properties were determined with an LR-100k universal testing machine (Lloyd Instruments, Ltd., West Sussex, United Kingdom) as per ASTM D 638.The test was performed with type-V tensile dumbbells with dimensions of 63.5 × 12.7 × 3 mm$^3$ at a crosshead speed of 5 mm/min and with a gauge length of 50 mm. The Izod impact strength was measured with impactometer (Ceast, Torino, Italy) as per ASTM D 256. Specimens with dimensions of 63.5 × 12.7 × 3 mm$^3$ with a notch angle of 45° and a depth of 2.54 mm were taken for measurement of the impact strength. Five samples were taken for the investigation of the tensile and impact properties.

### Dynamic mechanical analysis (DMA)

The viscoelastic properties, such as the storage modulus ($E'$), loss modulus ($E''$), and mechanical damping parameter (tan $\delta$), were measured as functions of the temperature with a dynamic mechanical thermal analyzer (Q800 TA Instruments, Delware, USA) at a fixed frequency of 1 Hz and at a heating rate of 2°C/min. Samples with dimensions of 55 × 12.7 × 3.17 mm$^3$ were taken for analysis under a nitrogen atmosphere over a temperature of −150 to 150°C in three-point-bending mode.

**TABLE I**
**Mechanical Properties of the PTT/PP Blends**

| Blend ratio | Tensile modulus (MPa) | Tensile strength (MPa) | Impact strength (J/m) |
|---|---|---|---|
| PTT | 520.7 ± 20 | 51.13 ± 3 | 40.10 ± 5 |
| PP | 317.08 ± 18.5 | 26.65 ± 5 | 60.0 ± 5 |
| PTT/PP (90 : 10) | 607.05 ± 21 | 35.31 ± 2.5 | 41.17 ± 3.5 |
| PTT/PP (80 : 20) | 721.37 ± 24 | 45.38 ± 5 | 54.09 ± 2 |
| PTT/PP (70 : 30) | 697.65 ± 10.5 | 39.22 ± 4 | 43.06 ± 3 |
| PTT/PP (50 : 50) | 540.61 ± 12.8 | 37.40 ± 3.5 | 46.19 ± 4.6 |
| PTT/PP (30 : 70) | 457.41 ± 14 | 21.23 ± 2 | 42.03 ± 2.8 |

### Thermal analysis

Differential scanning calorimetry (DSC) measurements were carried with Diamond DSC equipment (PerkinElmer, Massachusetts, USA). The samples were scanned from 30 to 250°C at a rate of 20°C/min. Subsequently, the samples were held at 250°C for 5 min and then cooled from 250 to −30°C at 20°C/min. The corresponding melting temperatures, crystallization temperatures, and glass-transition temperatures ($T_g$'s) of the samples were noted. The thermal stability in the samples was studied from thermogravimetric analysis (TGA) thermograms with a Pyris-7 TGA instrument (PerkinElmer). Samples of about 10 mg were heated from 50 to 700°C at a heating rate of 20°C/min in a nitrogen atmosphere, and the corresponding degradation temperature and percentage ash content were noted.

## RESULTS AND DISCUSSION

### Mechanical properties

#### Effect of the incorporation of PP on the mechanical properties of the PTT/PP blends

The variation of the impact strength of PTT as a function of the PP loading is depicted in Table I. It was evident that incorporation of PP resulted in a considerable increase in the Izod impact strength of the PTT/PP blend. The blend prepared at a PTT/PP ratio of 80 : 20 exhibited optimum performance compared with virgin PTT. An increase in the impact strength to the tune of 34.88% compared with virgin PTT was observed. This behavior was due to the fact that both PTT and PP were semicrystalline polymers, and the molecular weight of PP was considerably higher and, thereby, contributed to an increase in the impact strength of the PTT matrix. Similar improvements in the impact strength of the PTT matrix have been also reported for several other systems, such as PTT/EPDM (Ethylene propylene diene monomer) and PTT/m-LLDPE (metallocene-Linear low density polyethylene).[16,17] However, PTT and PP both formed immiscible blends; hence, the resultant improvement in the impact strength was not very significant. Moreover, with further increases in the PP content beyond 20 wt %, there was a decline in the impact strength of the blends; this was probably due to the increase in the domain size of the dispersed phase, which resulted in the coarsening of the PP domains at higher concentrations and led to coalescence.[18,19]

A similar trend was also observed for the tensile properties. The tensile modulus of PTT also increased with the addition of PP. The PTT/PP blend at a PP content of 20 wt % exhibited the maximum tensile modulus. The test results reported in Table I show that the tensile modulus of PTT increased from 520.7 ± 20 to 721.37 ± 24 MPa in the PTT/PP blend at 80 : 20 ratios; this was mainly because both PTT and PP had good tensile moduli; this resulted in an improvement in the modulus of the blend. Furthermore, PTT, being polar, and PP, being nonpolar in nature, showed some miscibility characteristics in the blend. However, beyond 20 wt % PP, there was a similar reduction in the tensile modulus to that observed in the case of the impact strength of the blend. This behavior was primarily attributed to the poor dispersion of PP domains within the PTT matrix, which increased the incompatibility between both phases. On the contrary, the blend prepared at an 80 : 20 ratio of PTT to PP showed a marginal miscibility window; this resulted in a good dispersion of PP within the PTT matrix. Further addition of PP in the blend matrix also increased the crystallinity of the blend; this might have contributed to an increase in the tensile modulus. Conversely, the tensile strength of the blend decreased at all compositions compared to virgin PTT, at all ratios of PTT to PP; this further confirmed the formation of an immiscible phase.

Because the blend prepared at an 80 : 20 ratio of PTT to PP exhibited the optimum impact strength, this composition was maintained for further investigations of the blend nanocomposite systems.

#### Effect of the compatibilizer on the mechanical properties of the PTT/PP blends

This compatibilization strategy involved the improvement of the interaction balance between PTT with a second immiscible phase, PP, by the introduction of a reactive compatibilizer, MAPP, which was

**TABLE II**
**Mechanical Properties of the Compatibilized PTT/PP Blends**

| Blend composition | Tensile modulus (MPa) | Tensile strength (MPa) | Impact strength (J/m) |
|---|---|---|---|
| PTT/PP (80 : 20) | 721.37 ± 24 | 45.38 ± 5 | 54.09 ± 2 |
| PTT/PP (80 : 20)/5 wt % MAPP | 894.8 ± 19 | 46.92 ± 4.5 | 59.96 ± 4 |
| PTT : PP (70 : 30) | 697.65 ± 10.5 | 39.22 ± 4 | 43.06 ± 3 |
| PTT/PP (70 : 30)/5 wt % MAPP | 722.30 ± 18.5 | 41.02 ± 3.6 | 48.94 ± 3.5 |
| PTT/PP (30 : 70) | 457.41 ± 14 | 21.23 ± 2 | 42.03 ± 2.8 |
| PTT/PP (30 : 70)/5 wt % MAPP | 438.69 ± 16.5 | 24.86 ± 3.5 | 46.93 ± 2.7 |

physically immiscible with the second phase (PP) but had chemical functionality (anhydride group) and could react with the hydroxyl end group of PTT to form a graft copolymer at the interface. MAPP was used as a reactive compatibilizer precursor in this study. The possibility of the formation of a graft copolymer via ester bonding at the interface was investigated. Similar reactions of the hydroxyl groups of polyester with anhydrides were also reported by Hu and Lindt[20] and Marquez et al.[21] Also, intermolecular dipole–dipole interactions and interchange reactions between —OH, —COOH, and ester groups in the case of maleic anhydride modified polymers and polyesters were reported by various authors.[20,21]

PTT and PP are incompatible in blends. PTT is polar in nature, whereas PP is nonpolar. So, to enhance the compatibility of these two polymers, 5 wt % MAPP was used as a reactive compatibilizer. As mentioned previously, the anhydride group of MAPP reacts with the carboxylic group of PTT to form ester bonds. The variations in the mechanical properties of the blends after the addition of MAPP are depicted in Table II.

The blend compositions prepared at 80 : 20, 70 : 30, and 30 : 70 ratios of PTT to PP were used for the compatibilization with MAPP. The test results reported in Table II show that PTT/PP at an 80 : 20 blend ratio showed an optimum value of Izod impact strength of 59.94 ± 4 J/m. There was an increase of 10.85% in the impact strength compared to the blend at the same ratio. This increase in impact strength was primarily due to the improved dispersion of PP within the PTT matrix. The incorporation of MAPP reduced the particle size of PP and enhanced the compatibility at the interphase. The reduction in the particle size with the addition of the functionalized PP was also due to the stabilization of the blend morphology by the graft copolymer (MAPP) formed during melt mixing. The graft copolymer reduced the interfacial tension and suppressed the coalescence behavior. In addition, the presence of a graft copolymer at the blend interface broadened the interfacial region through the penetration of the copolymer chain segments into corresponding adjacent phases.[22]

The tensile properties of the compatibilized blend are also depicted in Table II. At 5 wt % MAPP, we observed an increase of 24.04% in the tensile modulus in the compatibilized PTT/PP blend compared with the blend matrix at a blend ratio of 80.20. This behavior was probably due to the fact that PP was inherently stiff and the incorporation of PP resulted in an increase in the crystallinity of the virgin polymer with a consequent increase in tensile modulus. The addition of MAPP to the blend also reduced the interfacial energy of both phases and, thereby, increased the compatibility. Interestingly, 5 wt % graft polymer was sufficient for interfacial saturation.[23,24] The equilibrium concentration of MAPP, at which the domain size leveled off, is called the *critical micelle concentration,* that is, the concentration above which micelles are formed. The interfacial tension was directly proportional to domain size.[25,26] The interparticle distance between the domains and domain size is enumerated in a later section.

Conversely, a decrease in the tensile strength of the blend was also observed, regardless of the addition of MAPP. This reduction in the tensile strength revealed the inherently weak strength of PP as compared with PTT; this has been widely reported by various authors for blends of polyesters with semicrystalline polyolefins.[27–29]

### Effect of the clay loading on the mechanical properties of the PTT/PP blends

On the basis of the impact and tensile properties, 5 wt % MAPP compatibilized PTT/PP with an 80 : 20 blend ratio was optimal. The mechanical properties of the PTT/PP blend nanocomposite with 3 wt % organically modified nanoclay are depicted in Table III.

The test results reported in Table III reveal that the impact strength increased to the tune of 14.8% in PTT/PP/MAPP/C20A and 20.22% in PTT/PP/MAPP/C30B at a clay loading of 3 wt % compared with the PTT/PP blend matrix. MAPP not only improved the miscibility between PTT and PP but also aided in expanding the clay galleries and enabling the insertion of polymer chains, which led to the formation of an intercalated nanocomposite structure. The intercalation occurred between the

**TABLE III**
**Effect of the Clay Loading on the Mechanical Properties of the PTT/PP Blends**

| Blend composition | Tensile modulus (MPa) | Tensile strength (MPa) | Impact strength (J/m) |
|---|---|---|---|
| PTT/PP (80 : 20)/5 wt % MAPP | 894.8 ± 19 | 46.92 ± 4.5 | 59.96 ± 4 |
| PTT/PP (80 : 20)/5 wt % MAPP/3 wt % C20A | 810.65 ± 15.5 | 49.23 ± 2.3 | 62.00 ± 3 |
| PTT/PP (80 : 20)/5 wt % MAPP/3 wt % C30B | 945 ± 18.40 | 52.60 ± 3 | 65.03 ± 4.8 |

aliphatic tallow of the quaternary ammonium salt of the organically modified clays (C20A and C30B) and the polar groups of PTT. The blend nanocomposite prepared with C30B nanoclay exhibited optimum impact strength compared with that of the C20A-based blend nanocomposite system. This was probably due to the fact that C30 B was polar in nature with two hydroxyl groups in its structure, which interacted more easily with the carboxyl groups of PTT. Hence, we assumed that within the blend matrix, C30B nanoclay was distributed predominantly in the PTT phase. On the other hand, C20A was nonpolar and offered more a hydrophobic character with its two hydrogenated tallow groups and one methyl group. This resulted in less compatibility with the PTT matrix, which ultimately contributed to less enhancement in the properties.

The tensile properties of the compatibilized blend and the nanocomposite are also depicted in Table III. It was evident that the tensile modulus and tensile strength of the blends increased with the addition of 3 wt % C20A and C30B nanoclays. The tensile strength of the blend matrix increased from 46.92 ± 4.5 to 49.23 ± 2.3 MPa in C20A and to 52.60 ± 3 MPa in the C30B blend nanocomposites; this indicated a stiffening effect of the nanoclay layers within the blend matrix. Similar linear increases in the tensile modulus to the tune of 80.95% in C20A and 94% in C30B were also obtained compared to that in the blend matrix. The tensile properties in a polymer blend are largely dependent on the composition, chemical structure, and level of dispersion. The presence of nanoclay helped to control the morphology of the blend by reducing the particle size of PP and, thus, increasing the dispersability within the PTT matrix; this was evident from the SEM micrographs discussed in later sections.

The incorporation of MAPP further reduced the interfacial energy of both phases and provided a reactive site for the intercalation of C20A and C30B. In the optimized compatibilized blend, the addition of C30B showed better tensile properties compared to the blend matrix. This enhancement in the tensile modulus and tensile strength was due to the reduction in molecular chain mobility. The differences in the chemical structure and the organic modifier used in the nanoclay played vital roles in the dispersion of layered silicates within the blend matrix. The mechanical performance of the blend and blend nanocomposites varied in the following order:

PTT/PP/MAPP/C30B > PTT/PP/MAPP/C20A > PTT/PP/MAPP > PTT/PP

## DMA

DMA measures the stiffness and mechanical damping or internal friction/thermal dissipation of a deformed material as a function of temperature. The dynamic mechanical properties of the PTT/PP blend and the nanocomposites are depicted in Figures 1 and 2, respectively.

Figure 1 displays the $E'$–temperature curve of the virgin matrix PTT, PP, PTT/PP blend, and blend nanocomposites. It was evident that $E'$ of all of the samples decreased with increasing temperature. The incorporation of PP within the PTT matrix at an 80 : 20 ratio resulted in a decrease in $E'$ of the matrix; this further revealed characteristics of an immiscible blend. However, the reactive compatibilization of the PTT/PP blend with MAPP increased $E'$ of the PTT matrix considerably. There was a significant

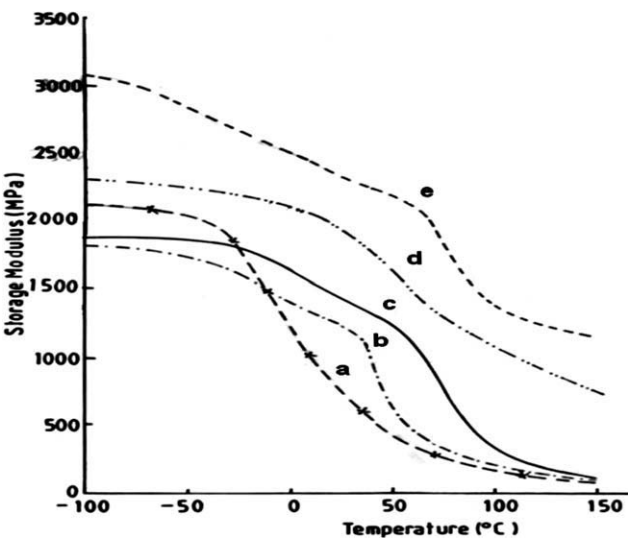


**Figure 1** Temperature dependence of $E'$ at 1 Hz for (a) PTT, (b) PP, (c) PTT/PP (80 : 20), (d) PTT/PP (80 : 20)/5 wt % MAPP, and (e) PTT/PP (80 : 20)/5 wt % MAPP/3 wt % C30B.

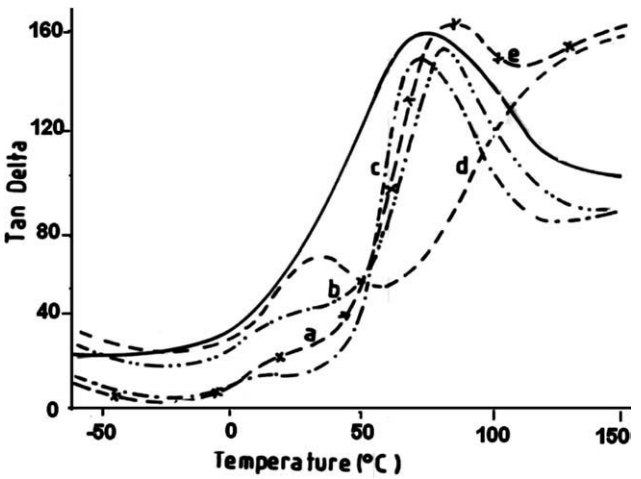


**Figure 2** Temperature dependence of tan δ at 1 Hz for (a) PTT, (b) PP, (c) PTT/PP (80 : 20), (d) PTT/PP (80 : 20)/5 wt % MAPP, and (e) PTT/PP (80 : 20)/5 wt % MAPP/3 wt % C30B.

increase in the matrix modulus from −50 to 75°C, beyond which $E'$ became comparable to that of virgin PTT. Further incorporation of organically modified nanoclay resulted in a significant increase in $E'$ of the blend matrix within the experimentally investigated temperature range. This phenomenon was primarily due to a reinforcing effect of the nanoscale platelets, which contributed to an effective stress transfer from the filler to the matrix at the interface.

The tan δ versus temperature plots of the virgin matrix PTT, PP, and its blends and blend nanocomposites are shown in Figure 2. It was evident that the tan δ curve of PTT and the PP matrix displayed only single peaks, corresponding to their glass transitions at 76.36 and 30.52°C, respectively. On the other hand, the blends and blend nanocomposites displayed two distinct peaks associated with the $T_g$ of the PP phase at 10.65°C and the $T_g$ of the PTT phase at 70.88C°; these indicated typical characteristics of an immiscible blend (Table IV). However, the $T_g$ of the PTT phase in the blend system was reduced in the presence of the PP phase because of the segmental immobilization of the PTT chains with the PP phase. Further, PP showed a high-temperature α-relaxation peak, which corresponded to the slippage of crystallites.

Conversely, the incorporation of MAPP to the blend matrix shifted the characteristic $T_g$'s of PP and the PTT phase to higher temperatures at 22.57 and 97.11°C, respectively; this indicated improved interfacial adhesion with compatibilization. Furthermore, the addition of the organoclay resulted in an additional shift in the $T_g$ of the blend matrix to higher temperature regions as compared to virgin PTT; this indicated the reinforcing effect of the organoclay, which restricted the segmental motion of the matrix chain.

However, the PTT/PP blends with and without MAPP and its blend nanocomposites exhibited two distinct transitions and revealed typical characteristics of incompatible blends.

## Morphology

The morphology of a blend strongly influences its ultimate properties. The morphology of a heterogeneous polymer blend, in fact, depends on the blend ratio, interfacial tension between the component polymers, and shear history during processing. The final morphology of a polymer blend depends on the balance of the domain breakup and coalescence at the end of the mixing process.[30,31]

Figure 3 depicts SEM micrographs of the PTT/PP blends at a blend ratio of 80 : 20 at three different magnifications. It was evident that the nonpolar PP phase was dispersed randomly within the polar PTT matrix. The micrograph reveals a two-phase morphology with larger PP domains embedded within the continuous PTT matrix. This further confirmed phase separation at the interface with a high extent of debonding and void formation. The SEM micrograph of the compatibilized PTT/PP blends at a PTT/PP/MAPP ratio of 80 : 20:5 wt % is displayed in Figure 4. Compatibilization is a well-established route for enhancing the adhesion and reducing interfacial tension between phases in immiscible PTT/PP blends. We inferred from this figure that the droplet size of the dispersed-phase PP decreased with the addition of 5 wt % MAPP as a reactive

**TABLE IV**
**$T_g$ and Tan δ Values of PTT and PP in the Blend and Its Nanocomposites**

| Sample | $T_g$ (°C) | | Tan δ | |
|---|---|---|---|---|
| | PTT | PP | PTT | PP |
| PTT | 76.36 | — | 0.1523 | — |
| PP | — | 30.52 | — | 0.07269 |
| PTT/PP (80 : 20) | 70.88 | 10.65 | 0.1451 | 0.03251 |
| PTT/PP (80 : 20)/5 wt % MAPP | 97.11 | 22.57 | 0.1272 | 0.04802 |
| PTT/PP (80 : 20)/5 wt % MAPP/3 wt % C30B | 94.46 | 16.13 | 0.1347 | 0.03430 |

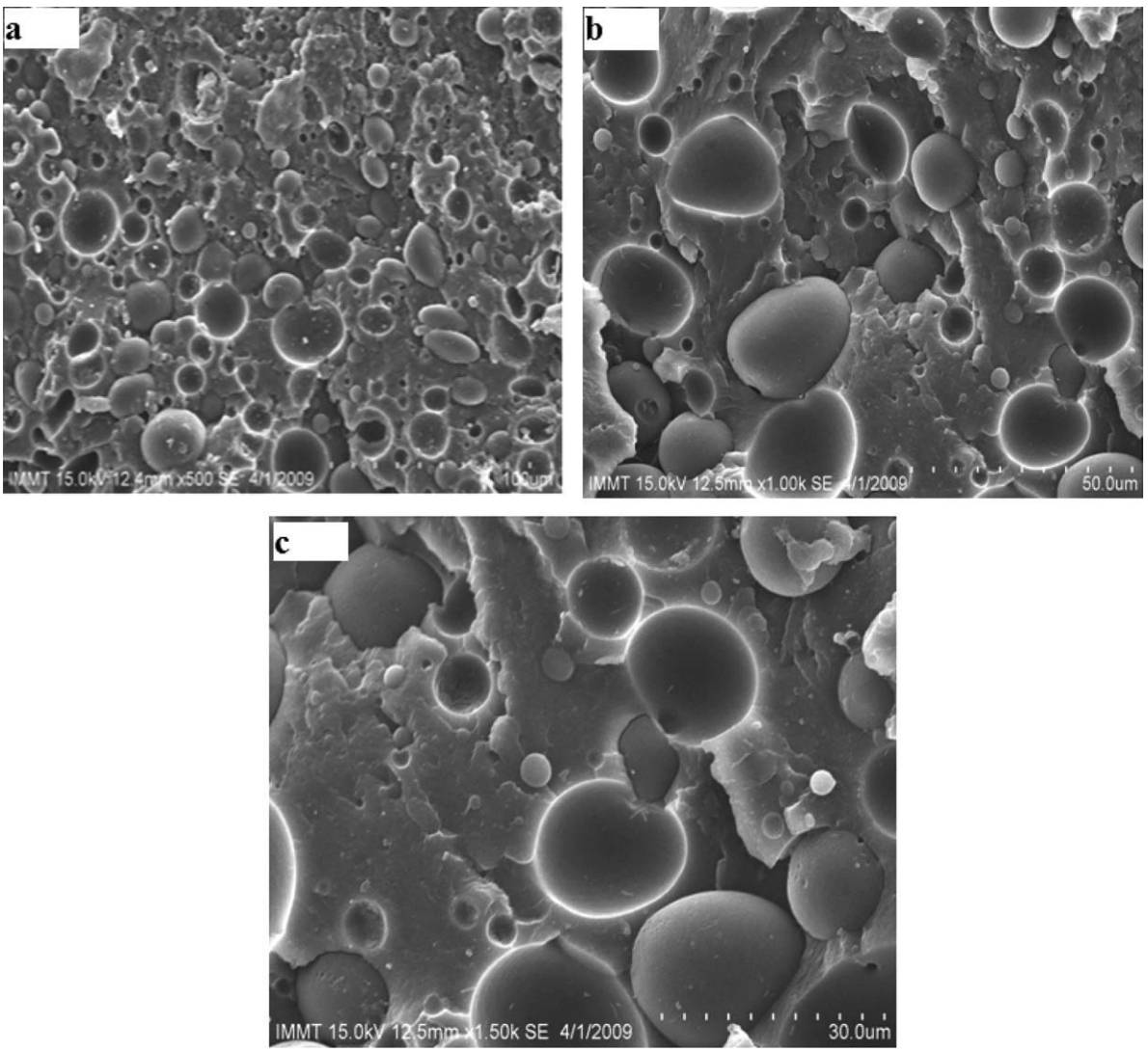


**Figure 3** SEM micrographs of the PTT/PP (80 : 20) blend at three different magnifications (500, 1000, and 1500×).

compatibilizer. This reduction in droplet size may have been due to the formation of a genuine interface, which resulted from the migration of MAPP to the boundary zone area between the two polymers, which anchored along the interface and interacted with the latter; this led to a decline in the interfacial tension.

Further, the particle size of the PP domains was measured in the representative zones of the cryogenically fractured impact specimens. The weight-average particle size ($d_w$) was calculated from approximately 200 particles as follows:

$$d_w = \frac{\sum nd^2}{\sum nd} \tag{1}$$

where $n$ is the number of particles of size $d$. The average interparticle distance ($\tau$) was calculated with the following equation:

$$\tau = d\left[k(\Pi/6\varphi)^{1/3} - 1\right] \tag{2}$$

where $\varphi$ is the volume fraction of PP and $k$ is a geometric constant (equal to 1 for a cubic lattice).

With the previous equation, the interparticle distance in the PTT/PP (80 : 20) blend matrix was found to be 3.33 μm. Furthermore, the particle size in the blend matrix decreased to 1.27 μm on reactive compatibilization; this reduced the interfacial tension with the interaction between the anhydride groups of MAPP and the hydroxyl groups of PTT.

Figure 5 shows the WAXD pattern of the 3 wt % C20A and C30B PTT/PP blend nanocomposites. The XRD pattern of the modified clay revealed reflection peaks at $2\theta = 3.65$ and 4.7° with $d$-spacings of 2.42 and 1.85 nm, respectively. The C20A nanoclay exhibited maximum basal spacing, which was probably due to the difference in the structure of the intercalants used in the modification.[32] C20A constitutes a

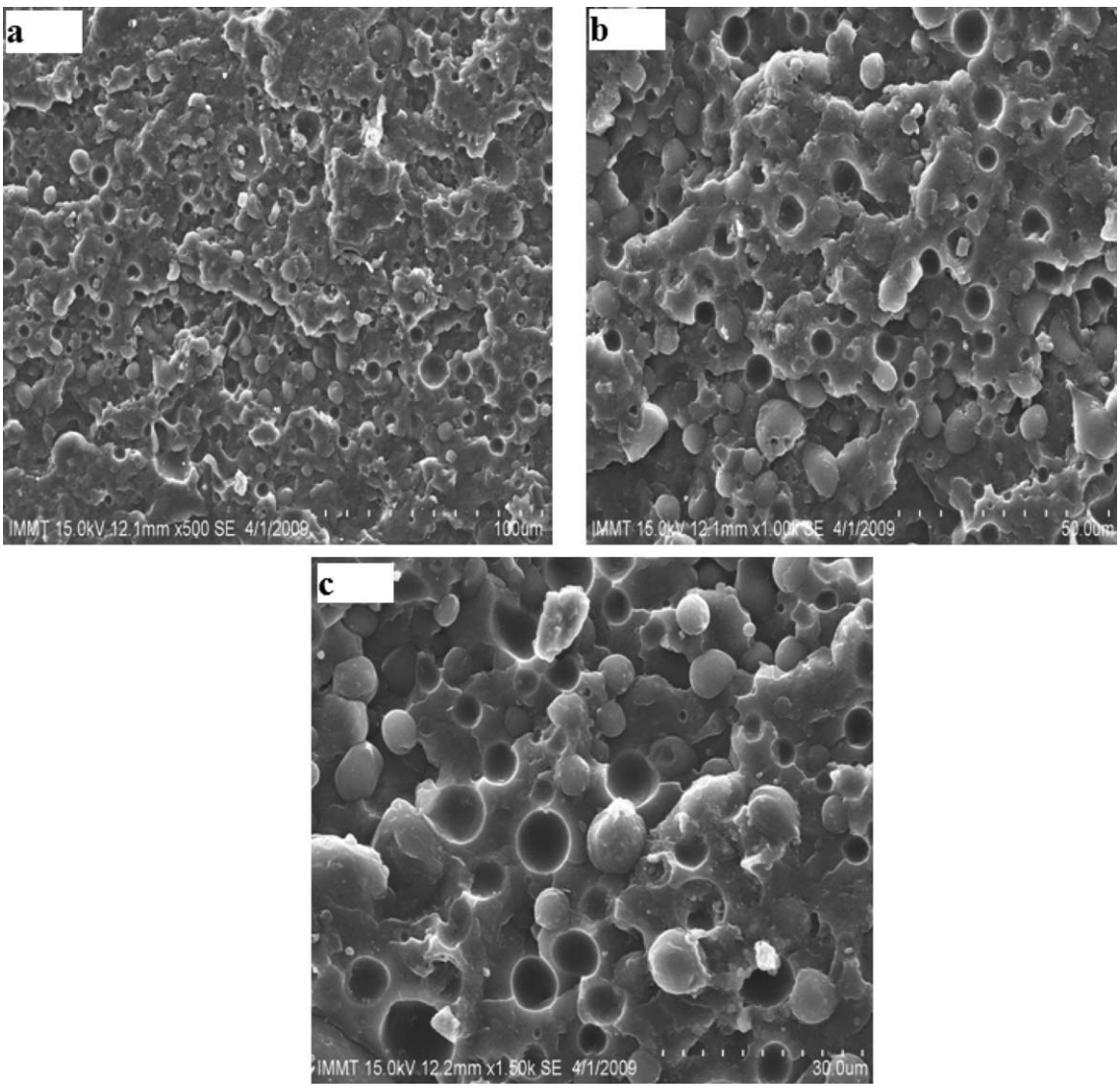


**Figure 4** SEM micrographs of the PTT/PP (80 : 20)/5 wt % MAPP blend at three different magnifications (500, 1000, and 1500×).

quaternary ammonium salt containing two alkyl hydrogenated tallow units along with a methyl group on the nitrogen atom. The initial value of the organoclay basal spacing is presented in Table V.

The X-ray diffraction patterns of the blend nanocomposites prepared with the C20A and C30B nanoclays at 3 wt % loading are also displayed in Figure 5. The $d_{001}$ plane diffraction peak of the PTT/PP blend nanocomposite with C20A and C30B shifted to a lower angle; this suggested that the PTT/PP chains were intercalated into the clay layers. The intercalation of the polymer chains led to decreased entropy in the system with a simultaneous increase in the conformational freedom of the surfactant molecules; thereby, this compensated for the overall entropy lost during separation of the silicate galleries.

As shown in Figure 5, the PTT/PP/C20A blend nanocomposites exhibited a diffraction peak at $2\theta = 2.3^\circ$ to a *d*-spacing of 3.8 nm. Similarly, the PTT/PP/C30B blend nanocomposites also showed a *d*-spacing of 4.16 nm with $2\theta = 2.16^\circ$

The presence of MAPP as a compatibilizer to the tune of 5 wt % also facilitated the expansion of gallery space of the nanolayers by the inclusion of polar maleic anhydride groups, which intercalated between the silicate layers. Hydrogen bonding between the oxygen atom of the silicate tetrahedra and the anhydride group of MAPP enhanced the interlayer distance of the stacked nanolayers and, thereby, resulted in the efficient dispersion of nanoparticles within the PTT/PP blend matrix. However, in the both the blend nanocomposites systems, diffraction peaks at $2\theta = 5.7^\circ$ (for PTT/PP/C30B) and $4.42^\circ$ (for PTT/PP/C20A) were observed. This indicated that some part of the clays remained in an agglomerated form within the blend matrix.

The maximum change in *d*-spacing was observed in the blend nanocomposite containing C30B

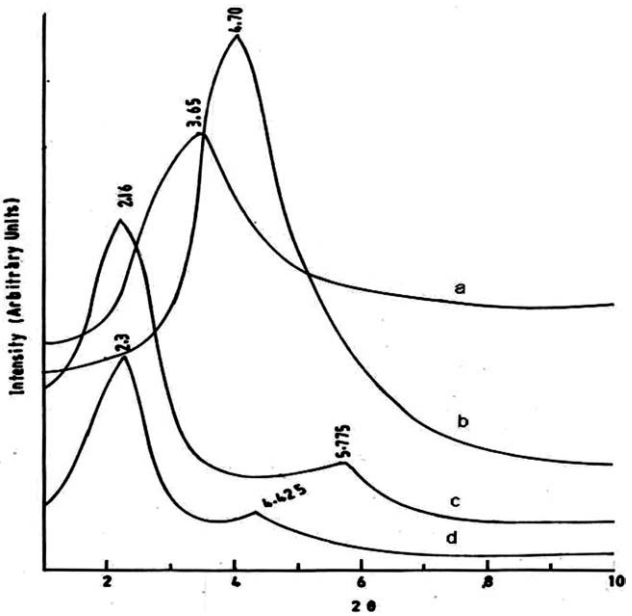


**Figure 5** WAXD patterns of (a) C20A, (b) C30B, (c) PTT/PP (80 : 20)/5 wt % MAPP/3 wt % C20A, and (d) PTT/PP (80 : 20)/5 wt % MAPP/3 wt % C30B.

nanoclay. The percentage increases in the *d*-spacing of C20A and C30B were 57 and 124%, respectively; this further confirmed effective interaction between the PTT/PP blend matrix and the C30B nanoclay due to strong hydrogen bonding between the carboxylic group of PTT and the —OH group of the organomodified galleries of C30B.

To determine the structure of the blend and blend nanocomposites, FTIR measurements were carried out. Figure 6 shows the FTIR spectra of PTT/PP (80 : 20)/5 wt % MAPP, PTT/PP (80 : 20)/3 wt % C20A and 3 wt % C30B, respectively. The peak at 1462.4 $cm^{-1}$ was attributed to the special vibration of the methylene group of PTT. The peak at 1708.5 $cm^{-1}$ represented the stretching vibration of C=O in the ester linkage of PTT, whereas the peak corresponding to 720.8 $cm^{-1}$ was due to the interfacial swinging vibration of the three methylene ($—CH_3$) groups. Peaks around 1240 and 1504 $cm^{-1}$ were assigned to the stretching vibration of the C—O in the carboxyl group and the characteristic absorption of the phenyl group.[33] The bands at 2870 and 2950 $cm^{-1}$ were assigned to the stretching vibration of the $—CH_3$ group of PP, and that at 2917 $cm^{-1}$ was attributed to the $—CH_2$ group of PP. Similarly, the band at 1462.5 $cm^{-1}$ was also assigned to the $CH_3$ or $CH_2$ group of PP.

Although the PTT/PP blend was compatibilized with MAPP, we did not observe any absorption band at 1712 $cm^{-1}$ (carboxylic acid) or 1780 or 1850 $cm^{-1}$ (anhydride) corresponding to the anhydride group. This may have been due to the fact that the content of MAPP was too low (5 wt %) to represent any characteristics peak in the spectrum.[34]

Furthermore, with the incorporation of 3 wt % C20A or C30B, the compatibilized PTT/PP blend displayed a peak at 1038 $cm^{-1}$ assigned to the Si—O stretching peak and a band at 460.1 $cm^{-1}$ corresponding to the Si—O bending peak of the organoclays.

TEM provided the dispersion characteristics of the clays in the PTT/PP blend matrix. Figure 7 shows a TEM image of the PTT/PP/MAPP/C30B (80 : 20:5 : 3) blend nanocomposites. The deep gray dispersed domains correspond to the PP phase. The gray domains correspond to the PTT matrix, and the black line corresponds to clay platelets. It was evident that clay monolayers or several layers were homogeneously dispersed in the blend matrix; this confirmed the formation of an intercalated structure in the nanocomposites. Because the clays platelets were dispersed in both the domains of PTT and PP in the presence of MAPP, the same was also assumed to improve the compatibility in the PTT/PP blend.

## Thermal properties

Figure 8 shows the TGA results of the PTT, PP, and PTT/PP blend and blend nanocomposites. The virgin PTT exhibited an initial degradation temperature ($T_{id}$) of 352.12°C with a final degradation temperature ($T_{fd}$) 503.47°C, whereas virgin PP exhibited a $T_{id}$ value of 287.4°C and a $T_{fd}$ value of 518.2°C. The incorporation of the PP phase to the tune of 20 wt % within the PTT matrix increased $T_{id}$ of the PTT matrix from 352.12 to 443.88°C and $T_{fd}$ from 503.47 to 565.48°C, respectively. At 10 wt % loss, the PTT/PP blend showed higher $T_{id}$ and $T_{fd}$ values than virgin PTT. Similarly, at 50 wt % loss, the blend matrix showed an enhancement in the $T_{id}$ and $T_{fd}$ values;

**TABLE V**
**TGA of the PTT/PP Blends and Its Nanocomposites**

| Sample | $T_{id}$ (°C) | $T_{10}$ (°C) | $T_{50}$ (°C) | $T_{fd}$ (°C) | Ash content (%) |
|---|---|---|---|---|---|
| PTT | 352.120 | 376.47 | 401.474 | 503.47 | 0 |
| PP | 387.40 | 384.09 | 439.12 | 518.28 | 0 |
| PTT/PP (80 : 20) | 443.88 | 411.59 | 440.01 | 565.48 | 4.05 |
| PTT/PP (80 : 20)/5 wt % MAPP | 343.46 | 411.34 | 441.74 | 594.25 | 4.51 |
| PTT/PP (80 : 20)/5 wt % MAPP/3 wt % C30B | 317.34 | 411.80 | 444.56 | 577.59 | 4.75 |

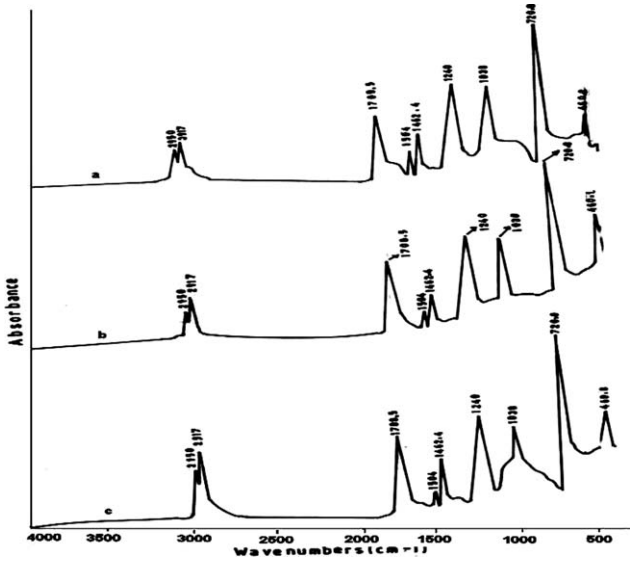


**Figure 6** FTIR spectra of (a) PTT/PP (80 : 20)/5 wt % MAPP, (b) PTT/PP (80 : 20)/5 wt % MAPP/3 wt % C20A, and (c) PTT/PP (80 : 20)/5 wt % MAPP/3 wt % C30B.

this indicated a higher thermal stability in the blend compared with the individual constituent polymers.

However, the addition of MAPP to the blend matrix decreased $T_{id}$ from 443.88 to 343.46°C and increased $T_{fd}$ from 565.48 to 594.25°C; this was probably due to the presence of a genuine interface.

Additionally, the presence of 5 wt % C30B organoclay substantially increased the thermal stability of the blend matrix [10% degradation temperature ($T_{10}$), 50% degradation temperature ($T_{50}$), and final degradation temperature ($T_{fd}$)], and this indicated a higher thermal stability due to the stable morphology of the dispersed phase and the presence of intercalated silicate layers, which might have contributed to the enhanced thermal stability of the blend nanocomposites. Furthermore, as discussed by Lim et al.,[35] the improvement in the thermal stability for polymer blend nanocomposites is primarily due to the formation of char, which hinders the outdiffusion of volatile decomposition products as a direct result of a decrease in the permeability.

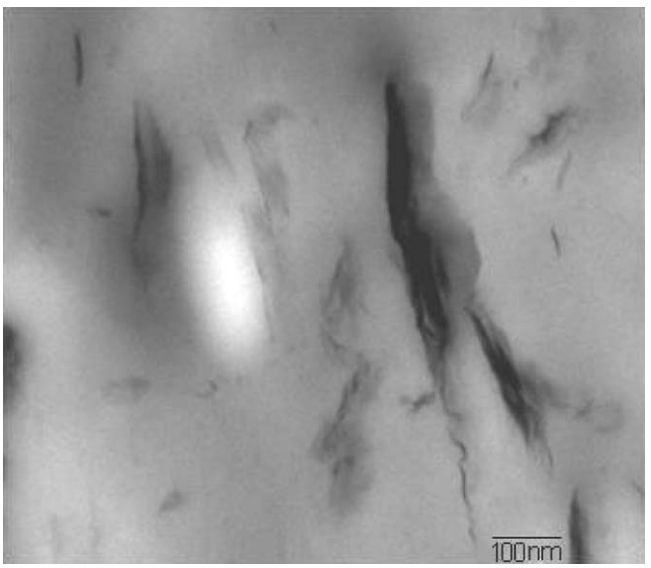


**Figure 7** TEM image of the PTT/PP/MAP/C30B (80 : 20:5 : 3) nanocomposites.

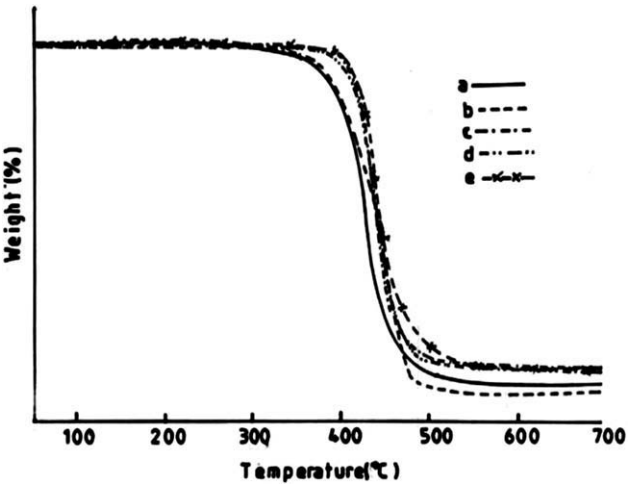


**Figure 8** TGA graphs of (a) PTT, (b) PP, (c) PTT/PP (80 : 20), (d) PTT/PP (80 : 20)/5 wt % MAPP, and (e) PTT/PP (80 : 20)/5 wt % MAPP/3 wt % C30B.

DSC thermograms of the virgin PTT, PP, PTT/PP blend, and the nanocomposites are enumerated in Figures 9 and 10. The corresponding crystallization temperature ($T_c$), melting temperature ($T_m$), heat of fusion ($H_m$), and degree of crystallinity ($X_c$) values are also presented in Table VI. The virgin PTT exhibited a $T_m$ of 228°C, whereas the PP matrix showed its corresponding $T_m$ around 164.82°C. In case of the

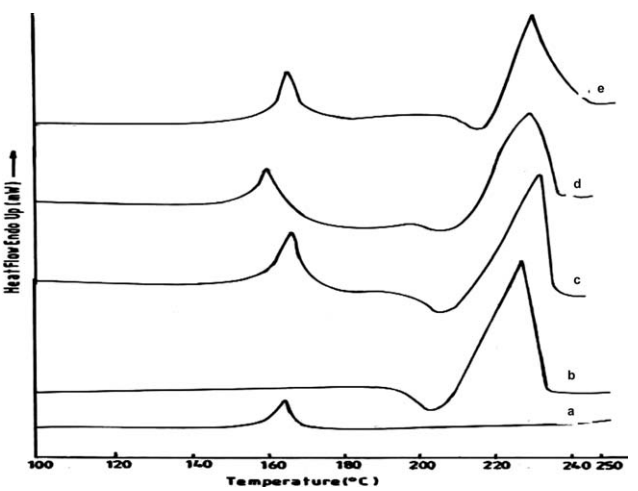


**Figure 9** DSC melting thermograms of (a) PP, (b) PTT, (c) PTT/PP (80 : 20), (d) PTT/PP (80 : 20)/5 wt % MAPP, and (e) PTT/PP (80 : 20)/5 wt % MAPP/3 wt % C30B.

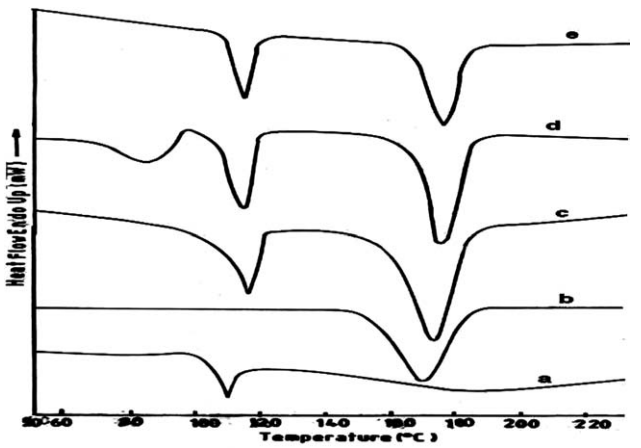


**Figure 10** DSC cooling thermograms of (a) PP, (b) PTT, (c) PTT/PP (80 : 20), (d) PTT/PP (80 : 20)/5 wt % MAPP, and (e) PTT/PP (80 : 20)/5 wt % MAPP/3 wt % C30B.

PTT/PP blend, two distinct melting endotherms were observed around 233.40 and 163°C, respectively. The presence of two melting peaks revealed characteristics of incompatible blends. Furthermore, with the addition of 5 wt % MAPP, the $T_m$ of both the PTT and PP phases decreased; this revealed the presence of an interface. Decreases in $T_m$ from 233.40 to 228.69°C in the PTT phase and from 163 to 161.27°C in the PP phase were observed.

On the contrary, in the blend nanocomposite, there was a marginal increase in $T_m$ of the PTT matrix from 228 to 229.32°C, whereas the PP phase did not show any effect, regardless of the addition of MAPP and clay. This indicated that the C30B clay preferentially resided within the PTT matrix.

Figure 10 shows the DSC cooling thermograms of the PTT, PP, PTT/PP blends, and the nanocomposites. The crystallization peak temperature ($T_c$) of virgin PTT was observed around 169.94°C; it increased considerably to 172.67°C with the incorporation of PP.

Similarly, $T_c$ of the blend matrix increased from 172.67 to 176°C with the addition of MAPP as a reactive compatibilizer. Additionally, $T_c$ of the blend matrix increased from 172.67 to 175.95°C in the presence of C30B organoclay. This confirmed that the silicate layers acted as a efficient nucleating agent for the crystallization of the PTT matrix. The extensive investigation of Maiti et al.[36] also showed that the degree of spherulite size was affected by the incorporation of organoclay content in PTT nanocomposites, which indicated that organoclay particles effectively act as nucleating agents. Nanoclays are assumed to be polar compounds with a high solubility parameter of 21.5 $(J/cm^3)^{1/2}$; hence, for polymers with a low solubility parameter, the polymer becomes incompatible with nanoclays; this results in the restriction of the polymer chains in the entering gallery space. In this context, PP with a low solubility parameter 15.4 $(J/cm^3)^{1/2}$ [37] did not allow the chains to enter the gallery of the clay. On the contrary, the solubility parameter of PTT ranged between 20.04 and 20.02 $(J/cm^3)^{1/2}$ as per group contribution theory, which matched with that of C30B, which was 21.5 $(J/cm^3)^{1/2}$. This fact might have contributed to enhanced compatibility of C30B.

## CONCLUSIONS

- PTT/PP blends with and without compatibilizer and nanocomposites were prepared with the melt-compounding technique.
- The incorporation of PP within the PTT matrix resulted in increases in the impact strength and tensile properties of the virgin matrix.
- Morphological observation (SEM) showed phase-separated morphologies in the PTT and PP phases in the blend matrix. WAXD analysis confirmed the efficient dispersion of nanoclays and the intercalation of the polymer segments in the gallery space in the organically modified nanocomposites. FTIR analysis confirmed the interactions among the PTT, PP, MAPP, and organoclay.
- DSC measurements revealed that the blend nanocomposite system displayed two distinct $T_m$'s; this revealed a phase-separated morphology. The incorporation of organically modified nanoclays increased the $T_c$ values of both the PTT and PP phases in the blend matrix. This indicated an improved compatibility of nanoclay in the PTT matrix.

**TABLE VI**
**Summary of the DSC Results of the PTT/PP Blend and Its Nanocomposites**

| Sample | $T_m$ (°C) | | $T_c$ (°C) | | $H_m$ (J/m) | | $X_c$ (%) | |
|---|---|---|---|---|---|---|---|---|
| | PP | PTT | PP | PTT | PP | PTT | PP | PTT |
| PTT | — | 228 | — | 169.94 | — | 58.302 | — | 39.93 |
| PTT/PP (80 : 20) | 163 | 233.40 | 115.93 | 172.67 | 8.388 | 51.185 | 80.0 | 43.82 |
| PTT/PP (80 : 20)/5 wt % MAPP | 161.27 | 228.69 | 114.88 | 176.28 | 38.524 | 60.580 | 31.74 | 51.86 |
| PTT/PP (80 : 20)/5 wt % MAPP/3 wt % C30B | 164.28 | 229.32 | 114.54 | 175.95 | 15.267 | 50.675 | 17.41 | 43.38 |
| PP | 164.82 | — | 106.57 | — | 41.879 | — | 17.43 | — |

- From the DSC and SEM micrographs, we confirmed that the PTT/PP blend was immiscible, although incorporation of MAPP slightly improved the blend compatibility.
- In the blend nanocomposites, $E'$ increased with the incorporation of the nanoclays. The tan $\delta$ of the blend matrix displayed two distinct transitions corresponding to PTT and PP.
- TGA thermograms also revealed a higher thermal stability of the blend matrix in the presence of nanoclays.
- For the rubber-toughened PTT (PTT/PP blend), a good balance of properties in terms of stiffness and strength was achieved at an optimal concentration of clays and MAPP.

## References


1. Mishra, S. P.; Deopure, L. Polym Bull 1985, 26, 5.
2. Yu, Y.; Choi, K. J. Polym Eng Sci 1997, 37, 91.
3. Nabisaheb, D.; Iog, J. P. J Polym Sci Part B: Polym Phys 1999, 37, 2439.
4. Avramova, N. Polymer 1995, 36, 801.
5. Utracki, L. A. Polymer Alloys and Blends: Thermodynamics and Rheology; Hanser: New York, 1990.
6. Fried, J. R. Text Book of Polymer Science and Technology; Prentice Hall of India: New Delhi, 2003.
7. Folkes, M. J.; Hope, P. S. Text Book of Polymer Blends and Alloy; Chapman & Hall: London, 1993.
8. Khatua, B. B.; Lee, D. J.; Kim, H. Y.; Kim, J. K. Macromolecules 2004, 37, 2454.
9. Ray, S. S.; Bousmina, M. Macromol Rapid Commun 2005, 26, 1639.
10. Lim, J. W.; Hassan, A.; Rahmat, A. R.; Wahit, M. U. Polym Int 2006, 55, 204.
11. Li, Y. J.; Shimizu, H. Polymer 2004, 45, 7381.
12. Li, Y. J.; Shimzu, H. Macromol Rapid Commun 2005, 26, 710.
13. Fena, M.; Gong, F. L. Polym Int 2004, 53, 1529.
14. Huang, X. Y.; Lewis, S.; Brittain, W. J.; Vaia, R. A. Polym Prepr 2000, 41, 589.
15. Huang, X. Y.; Lewis, S.; Brittain, W. J.; Vaia, R. A. Macromolecules 2000, 33, 2000.
16. Xue, M. L.; Yu, Y. L.; Chuah, H. H. Eur Polym J 2007, 43, 3826.
17. Aravind, I.; Albert, P. Polymer 2004, 45, 4925.
18. Allan, R. S.; Mansan, S. G. J Colloid Sci 1962, 17, 383.
19. Chem, J.; Hahn, P. S.; Slattery, J. C. AIChE J 1984, 30, 622.
20. Hu, G. H.; Lindt, T. J Polym Sci Part A: Polym Chem 1993, 31, 691.
21. Marquez, L.; Gambus, D. E.; Romero-Rato, M. P.; Sabino, M. A. Soc Plast Eng Annu Tech Conf 1999, 45, 3903.
22. Dedecker, K.; Groeninckx, G. Polymer 1998, 39, 4985.
23. Cinaga, P.; Favis, B. D.; Jerome, R. J Polym Sci 1990, 30, 1073.
24. Kim, S. J. K.; Kim, S.; Park, C. E. Polymer 1997, 38, 2155.
25. Roland, C. M.; Bohm, G. G. J Polym Sci Polym Phys Ed 1984, 22, 79.
26. McMaster, L. P. Adv Chem Ser 1975, 43, 142.
27. Guerrica, E. G.; Eguiazabal, J. I.; Nazabal, J. Polym Eng Sci 2006, 46, 172.
28. Khatua, B. B.; Lee, D. J.; Kim, H. Y.; Kim, J. K. Macromolecules 2004, 37, 2454.
29. Ray, S. S.; Bousmina, M. Macromol Rapid Commun 2005, 26, 1639.
30. Taylor, G. I. Proc R Soc London Ser A 1932, 138, 41.
31. Taylor, G. I. Proc R Soc London Ser A 1934, 146, 501.
32. Boyde, R. H. Polymer 1985, 56, 323.
33. Kim, K. J.; Bae, J. H.; Kim, Y. H. Polymer 2001, 42, 1023.
34. Philippart, J. L.; Sinturel, C.; Arnaud, R.; Gardette, J. L. Polym Degrad Stab 1999, 64, 213.
35. Lim, J. W.; Hassan, A.; Rahmat, A. R.; Wahit, M. U. Polym Int 2006, 55, 204.
36. Maiti, P.; Nam, P. H.; Okamoto, M.; Kotaka, T.; Hosegawa, N.; Usuki, A. Polym Eng Sci 2002, 42, 1864.
37. Van Krevelen, D. W. Properties of Polymers: Correlation with Chemical Structure; Elsevier: Amsterdam, 1972.